PCCP

Accepted Manuscript

ROYAL SOCIETY OF CHEMISTRY

www.rsc.org/pccp

Adsorption of sodium diclofenac on graphene: a combined experimental and theoretical study

I.M. Jauris[a], C.F. Matos[b], C. Saucier[c], E.C. Lima[c], A.J.G. Zarbin[b], S.B. Fagan[a], F.M. Machado[d] and I. Zanella[a,*]

[a]*Technological Sciences Area, UNIFRA. Santa Maria, RS, Brazil.*E-mail: ivanazanella@gmail.com.*

[b]*Chemistry Department, Federal University of Paraná, UFPR, Curitiba, PR, Brazil.*

[c]*Institute of Chemistry, Federal University of Rio Grande do Sul, UFRGS, Porto Alegre, RS, Brazil.*

[d]*Technology Development Center, Federal University of Pelotas, UFPEL, Pelotas, RS, Brazil.*

Abstract

The interaction of sodium diclofenac drug (s-DCF) with different graphene species was investigated using both first principles calculations based on Density Functional Theory (DFT) and adsorption experiments. Through batch adsorption experiments, it was found that the rGO was good adsorbent for removing s-DCF drug from aqueous solutions. The general-order kinetic model shows the best fit to the experimental data compared with pseudo-first order and pseudo-second order kinetic adsorption models. The equilibrium data (at 25 ^{o}C) was fitted to the Liu isotherm model. The maximum sorption capacity for adsorption of the s-DCF drug was 59.67 mg g^{-1} for rGO. The s-DCF adsorption on pristine graphene, graphene with a vacancy, reduced oxide graphene (rGO) and functionalized graphene nanoribbons were simulated providing a good understanding of the adsorption process of this molecule on graphene-family surfaces. The results predict a physisorption regime in all cases. Based on these results, the *ab initio* calculations and experimental adsorption point out that graphene-family are promising materials for extracting s-DCF from wastewater effluents.

Keywords: *graphene; adsorption; drugs; ab initio calculations; density functional theory; nonlinear isotherm fitting.*

1.Introduction

A large number of different classes of pharmaceuticals products are used annually worldwide. These are used in medicine, veterinary medicine and also employed as growth promoters in animal husbandry.[1] Many pharmaceuticals undergo structural changes inside the bodies of humans and animals, and the result of such process is the metabolites. Most of the organic compounds are metabolized before being excreted, others are only partially metabolized and another part, such as contrast agents are excreted completely unchanged in the environment.[2-3] It has been reported that some of these metabolites and transformation

products are not eliminated during sewage treatment and may enter the aquatic environment and eventually reach the drinking water supply.[4-5] Among numerous pharmaceuticals commonly detected in drinking water sources and wastewater effluents, stands out the diclofenac (DCF).[6-7] This non-steroidal anti-inflammatory drug is recommended as oral tablets or as a topical gel to reduce inflammation, pain and fever. The yearly consumption of DCF varies between 195 - 940 mg per inhabitant in different countries.[8] This high consumption justifies the regularly of detection of these drug in the effluents of wastewater treatment plants.[7] Despite the therapeutic benefits, this drug may potentially cause adverse effects on aquatic organisms[9] and on chronic exposure, can cause even hemodynamic changes and thyroid tumors in human.[10] In this context, there is an increasing demand for competent methods to remove pharmaceuticals from wastewater.[11-14] Among the various techniques currently proposed, adsorption process assumes great evidence, because of its high efficiency and simplicity.[15-17] This process transfers the contaminant from the effluent to a solid phase, which significantly decreases the bioavailability of the hazardous species to living organisms.[5,18]

Different adsorbents have been used for the removal of pharmaceuticals from aqueous solutions, especially those carbon-based.[10-14] Saucier *et al.*[11] demonstrated that activated carbon from cocoa shell could act as a good adsorbent in adsorbing sodium diclofenac (s-DCF) and nimesulide from aqueous solution. The maximum amounts of s-DCF and nimesulide adsorbed onto activated carbon ware 63.47 and 74.81 mg g^{-1} at 25°C, respectively. Álvarez *et al.*[12] used carbon xerogels in the removal of diclofenac from aqueous solutions and the higher extent of diclofenac adsorption, 80.0 mg g^{-1}, was obtained with a carbon xerogel treated with H_2SO_3, principally due to electronic interactions. Hu and Cheng[13] studied the adsorption of diclofenac on multi-walled carbon nanotubes treated with HNO_3 and found that a physisorption mechanism should take place between adsorbate-adsorbent and adsorption process is spontaneous and exothermic.

The graphene-family, such as, graphene, graphene oxide (GO) and reduced graphene oxide (rGO) are among the adsorbents that have been employed for the successful removal

of emerging contaminants from aqueous effluents.[19] These are attractive alternative because they possess nanometer size as well as appropriate textural properties.[20] The nanosized structures donate them some advantages in the adsorption process, for example high adsorption capacity, rapid equilibrium rates, effectiveness over a broad pH and temperature range[21-23]. The presence of vacancies and functional oxygen-containing groups in the basal plane of GO and rGO, assist in electrostatic interactions between adsorbates and adsorbents and hydrogen bonding, may also assist in the adsorption.[19,24-25] Besides these characteristics, the large number of π electrons delocalized make the graphene appropriate for environmental decontamination applications.[19] Indeed, the characteristic structures and electronic properties make them interact good with organic molecules, via non-covalent forces.[23]

Despite the great potential of graphene-family, to the best of our knowledge, there are few papers currently published in the literature reporting on the use of graphene-family for drugs removal from aqueous effluents.[10,19,21,24] Therefore, the use of graphene-family for drugs adsorption requires new studies on this topic. Recently, Nam *et al.*[10] investigated the adsorption of diclofenac and sulfamethoxazole on GO using adsorption experiments and molecular modeling. The authors found that adsorption of both drugs showed relatively low sorption capacity by graphite oxide, but it can be increased with the sonication of GO, due to dispersion of exfoliated GO sheets and the reduction of oxygen-containing functional groups on the GO. Furthermore, the authors observed that the main adsorption mechanism of the drugs on GO was due to π–π electron donor acceptor interactions and hydrophobic interactions.

In the present work we study in an innovative way, the interaction between s-DCF molecule with pristine graphene, graphene with a vacancy, rGO and functionalized graphene nanoribbons, using *ab initio* calculations based on DFT[26-27] aiming to understand the adsorption mechanism of this molecule on the carbon lattice. In addition, the ability of rGO to remove s-DCF from aqueous solutions was examined by adsorption batch process. The rGO used as nanoadsorbents for the removal of s-DCF from aqueous solutions was obtained by a

modified Hummers method.

2. Materials and Methods

2.1 Chemicals, reagents and solutions

Natural graphite flakes (Graflake 99580 - Nacional de Grafite, Brazil), sulfuric acid (Carlo Erba), potassium permanganate (Merck), hydrogen peroxide (Vetec), sodium borohydride (Merck) were used as receive. The diclofenac sodium (was supplied by Medchemexpress (New Jersey, USA) at 99% purity and used without purification.

All solutions were prepared using deionized water. A stock solution was prepared by dissolving the s-DCF in deionized water to a concentration of 5.0 g L^{-1}. Working solutions were obtained by diluting the stock solution to the required concentrations. To adjust the pH of the solutions, 0.1molL^{-1} sodium hydroxide or hydrochloric acid solutions were used. The pH of the solutions was measured using a Schott Lab 850 set pH meter.

2.2 Adsorbent

Reduced graphene oxide was obtained by a modified Hummers method.[28] In this procedure 60 mL of H_2SO_4 were added to 1.0 g of graphite. The mixture was maintained in an ice bath and strong magnetic stirring for 15 min. Thereafter, 3.5 g of $KMnO_4$ were added to the system, and the mixture was kept under strong magnetic stirring for 120 min without the ice bath. Followed by 120 mL of distilled water and finally 3 mL of H_2O_2 (30% v/v). The resulting solid (graphite oxide) was filtered, washed with 500 mL of deionized water, 250 mL of a HCl (10% v/v) solution, 250 mL ethanol, 250 mL of acetone and finally several times with distilled water until pH neutral and dried at 60°C. To obtain the rGO the graphite oxide (1 mg mL^{-1}) was exfoliated in an ultrasound probe (Cole Parmer CP505 - 20 kHz - 500 W) for 10 minutes. The resulting dispersion was centrifuged for 90 min (3000 rpm). To the supernatant, GO, was added sodium borohydride ($NaBH_4$) in a proportion of 10 mg per each milliliter of dispersion, the mixture was then refluxed for 3 hours. The resulting black solid (rGO) was

138 separated by filtration, washed several times with distilled water, and dried at 50°C.

139 The rGO nanoadsorbent was characterized by FT-IR vibrational spectroscopy using a
140 BRUKER spectrometer, model 70-vertex using an attenuated total reflectance mode
141 accessory (Pike Technologies). The Raman spectrum was obtained in a Renishaw Raman
142 Image spectrophotometer coupled to an optical microscope that focused the incident
143 radiation down to a spot of approximately 1μm. The laser used was Ar^+ (514.5 nm) with less
144 than 1mW of power. Thermogravimetric analyses (TGA) were carried out in SDT Q600
145 equipment (TA Instruments) under an atmosphere of synthetic air (White Martins, 100 mL
146 min^{-1}) at a heating rate of 5 $Kmin^{-1}$ from room temperature to 800°C. The specific surface
147 area of rGO was estimated using Brunauer–Emmett– Teller (BET) equation to adsorption of
148 N_2 (at -196°C), performed on an NOVA 1200 model QuantaChrom equipment. The
149 morphology of the nanoadsorbent was characterized by scanning electron microscopy (SEM)
150 using a Tescan equipment by field effect (FEG) with a voltage of 15 kV (the images were
151 obtained from samples deposited over a Si substrate), and the topography of rGO was
152 acquired using an atomic force microscope (AFM, Shimadzu SPM-9700) operating in
153 dynamic mode.

154

155 *2.3 Adsorption Studies*

156 A 20.0 mL of s-DCF solution (20.0 – 200.0 mg L^{-1}) was added to a 30.0 mg of rGO
157 nanoadsorbent in various 50.0mL Falcon tubes at different pH values (8.0–10.0). The
158 mixtures were agitated between 3 and 480 min inside a thermostatic shaker (150 rpm) at
159 298K. The mixtures were centrifuged for 5 min to separate the nanoadsorbent from the
160 pharmaceutical solutions. The s-DCF left in solution after adsorption were quantified at
161 maximum wavelength of 275 nm, using T90+ UV-VIS spectrophotometer (PG Instruments),
162 provided with quartz optical cells. The amount of s-DCF removed by the rGO and the
163 percentage of removal were calculated using of Eqs. (1) and (2), respectively:

164

$$q = \frac{(C_o - C_f)}{m}.V \quad (1)$$

and

$$\%\text{Removal} = 100 \times \frac{(C_o - C_f)}{C_o} \quad (2)$$

where q is the amount of s-DCF adsorbed by the adsorbent (mg g^{-1}); C_o is the initial s-DCF concentration in contact with the nanoadsorbent (mg L^{-1}); C_f is the pharmaceutical concentration after the batch adsorption process (mg L^{-1}); m is the mass of nanoadsorbent (g); and V is the volume of the pharmaceutical solution (L).

The general order, pseudo-first order and pseudo second-order kinetic models[15-16]were used to analyze the kinetic data. The respective mathematical expressions of these models are presented in Eqs. (3)–(5),

$$q_t = q_e - \frac{q_e}{\left[k_N (q_e)^{n-1}.t.(n-1)+1\right]^{1/(1-n)}} \quad (3)$$

$$q_t = q_e\left[1-\exp(-k_1.t)\right] \quad (4)$$

$$q_t = q_e - \frac{q_e}{\left[k_2 (q_e).t+1\right]} \quad (5)$$

where q_t is the amount of adsorbate adsorbed at time t (mg g^{-1}); q_e is the amount adsorbate adsorbed at the equilibrium (mg g^{-1}); t is the time of contact (min); n is the order of kinetic adsorption (n could be an integral or a fractional number); k_1 is the pseudo-first order rate constant (min^{-1}); k_2 is the pseudo-second order rate constant (g mg^{-1} min^{-1}); and k_N is the general-order constant rate [min^{-1}.(g mg^{-1})$^{n-1}$].

The equilibrium of adsorption was evaluated using the Freundlich,[29] Langmuir,[30] and Liu[31] isotherm models. The respective mathematical expressions of these models are presented in Eqs. (6)-(8).

$$q_e = K_F.C_e^{1/n_F} \quad (6)$$

$$q_e = \frac{Q_{max}.K_L.C_e}{1+(K_L.C_e)} \quad (7)$$

$$q_e = \frac{Q_{max}.(K_g.C_e)^{n_g}}{\left(1+(K_g.C_e)^{n_g}\right)} \quad (8)$$

where q_e is the amount drug adsorbed at equilibrium (mg g^{-1}); C_e is the s-DCF concentration at equilibrium (mg L^{-1}); Q_{max} is the maximum sorption capacity of the rGO (mg g^{-1}); K_L is the Langmuir equilibrium constant (L mg^{-1}); K_F is the Freundlich equilibrium constant [mg g^{-1}.(mg $L^{-1})^{-1/nF}$]; K_g is the Liu equilibrium constant (L mg^{-1}); n_F and n_g are the exponents of Freundlich and Liu model, respectively (dimensionless).

Additionally, in order to demonstrate the direct physic diclofenac adsorption on rGO, thermogravimetric analyzes were performed using the pristine rGO and s-DCF solids and the solid resulting (loaded adsorbent) after the separation process of a s-DCF solution (50.0 mg L^{-1}) added (at low surface coverage) to the rGO.

2.4 Statistical evaluation of the kinetic and isotherm parameters

The kinetic and equilibrium models were fitted by employing a nonlinear method, with successive interactions calculated by the method of Levenberg-Marquardt and interactions calculated by the Simplex method, using the nonlinear fitting facilities of the software Microcal Origin 9.0. In addition, the models were evaluated using a determination coefficient (R^2), an adjusted determination coefficient (R^2_{adj}) and residual standard deviation (SD) [32]. The SD is a measurement of the difference between the theoretical amount of pharmaceutical removed by the nanoadsorbent and the actual amount of pharmaceutical measured experimentally. Equations 9, 10 and 11 are the mathematical expressions of R^2, R^2_{adj} and SD, respectively.

$$R^2 = \left(\frac{\sum_i^n (q_{i,exp} - \bar{q}_{exp})^2 - \sum_i^n (q_{i,exp} - q_{i,\,model})^2}{\sum_i^n (q_{i,exp} - \bar{q}_{exp})^2} \right) \quad (9)$$

$$R^2_{adj}=\left\{1-\left[\left(1-R^2\right).\left(\frac{n_p-1}{n_p-p-1}\right)\right]\right\} \quad (10)$$

$$SD=\sqrt{\left(\frac{1}{n-p}\right).\sum_i^n (q_{i,exp}-q_{i,\ model})^2} \quad (11)$$

where $q_{i,\ model}$ is the individual theoretical value of q, $q_{i,exp}$ is the individual measured value of q, $\bar{q}_{exp}$ is the average of q experimentally measured, n is the number of experiments performed and p is the number of parameters of the fitted model [32]

2.5 Theoretical calculations

Electronic and structural properties of graphene-family interacting with diclofenac sodium drug, in different arrangements/structural conformations, were obtained via *ab initio* calculations based on density functional theory,[27] and implemented through SIESTA code.[33] Calculation parameters and approaches are similar to those used by Machado *et. al.,*[15]where the energy shift was 0,05eV, a local density approximation (LDA) was adopted to exchange and correlation term, core electrons were described by Troullier-Martins pseudopotetials[34] and a polarized double-zeta basis (DZP) used for the basis set.[33] A cutoff radius of 300 Ry was adopted for grid integration, 3x1x3 k-points was chosen to integration over the first Brillouin zone, and atoms positions have been optimized through conjugate gradient algorithm until residual forces was less than 0.05 eV $Å^{-1}$.[33]

Binding energies (E_b) between sodium diclofenac and graphene-family was calculated using the correction to bases superposition error (BSSE) according to standard equation (Eq 12).[35]

$$E_b = E\left[Grap + s\text{-}DCF\right] - \left(E\left[Grap + s\text{-}DCF_{ghost}\right] + E\left[Grap_{ghost} + s\text{-}DCF\right]\right) \quad (12)$$

where *E(Grap+ s-DCF)* is the total energy of the graphene plus s-DCF molecule, E(Grap + s-DCF_{ghost}) is the total energy of the isolated graphene and *E($Grap_{ghost}$+ s-DCF*) is the total energy of s-DCF molecule. Ghost superscript refers to the atomic basis placed on the molecule or graphene positions but without atomic potentials representing real atoms at

these positions. Also were employed periodic boundary conditions along XZ plane of graphene. Thus, for pristine graphene (144 C-atoms), graphene with functional groups (epoxy and hydroxyl) and graphene plus a vacancy, a supercell with dimensions of 25.93 x 20.0 x 14.97Å was chosen. As for graphene nanoribbons (with carboxyl and carbonyl functional groups) a supercell with dimensions of 25.73 x 20.0 x 25.0 Å was adopted. The values for distance (d_b) between the s-DCF drug molecule and a graphene-family were obtained from the shortest distance between an atom of graphene-family with s-DCF molecule.[15]

3.Results

3.1Characterizations of rGO used as nanoadsorbent

Figures 1a and 1b show, respectively, SEM and AFM images of the reduced graphene oxide. The rGO sheets, from 0.1 to 5.0 μm, are mainly in a single-layer state according to the AFM investigation (around 1 nm in height), one can see a smaller amount the presence to multilayers (~ 3.4 nm). In the FT-IR spectra of the GO and rGO (Figure 1c) are noted the presence of bands in 3570-3425 cm^{-1} (ν_{OH} C−OH), 3190 cm^{-1} (ν_{OH} of H_2O), 2962 ,2920, 2850 cm^{-1} (ν_{CH}), 1726 cm^{-1} ($\nu_{C=O}$ of COOH), 1625 cm^{-1} (δ_{OH} of H_2O), 1574 cm^{-1} ($\nu_{C=C}$), 1402 cm^{-1} (δ_{OH} de C-OH), 1220 cm^{-1} (ν_{C-O-C} of epoxide) e 1060 cm^{-1} (ν_{C-O}).[28] The presence of these functional groups provide the GO high negative charge density. This characteristic can damage adsorption of organic molecules with negative charge.[36,37] After the chemical reduction of graphene oxide, there is a significant intensities decrease of the bands related to the presence of oxygenated functional groups, such as the bands centered at 1730 and 1116 cm^{-1}, which disappeared almost completely. This processes result in the partial deoxygenation and the gradual decrease of the negative charge density of rGO.[38,39] These characteristics can favor the electro-static interactions as well as hydrogen bonds between negative charged drugs, such as s-DCF, and the surface of rGO. Thermogravimetric analysis (Figure 1d) presented three events of mass loss. The first from room temperature to nearly 100°C, is associated to the loss of adsorbed water in the

material; the second between 130 at 350 °C is related to the removal of oxygenated groups present in these samples, corroborating infrared spectroscopy data; and the third between 400 at 650 °C attributed to combustion of the carbon skeleton, showing the high thermal stability of this material.[40] The Raman spectrum (Figure 1e) shows characteristic bands of carbonaceous material, D (1343 cm^{-1}), G (1580 cm^{-1}) and G" (2687 cm^{-1}), showing a material containing defects, e.g. incomplete bonds and Stone-Wales defects (pentagons and heptagons) in the hexagonal carbon structure in rGO.[41]

The BET specific surface area of this rGO is 98 $cm^2\ g^{-1}$. The discrepancy of the surface area value obtained compared to the theoretical (~ 2000 $cm^2\ g^{-1}$) is related to incomplete exfoliation and aggregation during the reduction process due to van der Waals interaction between the graphene layers.[42]

For a better approach between experimental and theoretical data, these structural characteristic of the rGO were considered in some structures used on theoretical calculations.

3.2 Experimental Adsorption

3.2.1 Kinetic studies

Nonlinear pseudo-first order, pseudo-second order and general-order kinetic models were used to explain the kinetic of adsorption of s-DCF onto rGO adsorbent. Figure 2 shows the kinetic curves while Table 1 presents the fitting parameters of the kinetic models. Standard Deviation (*SD*) values explain the suitability of each nonlinear kinetic model. The bigger the deviation of the theoretical *q* value from the experimental *q* value, the higher the *SD* value.[5, 11, 16, 18, 32] The *SD* of the minimum value was used to divide *SD* of each model (*SD* ratio) to compare the fitness of each model. General-order kinetic model has the lowest *SD* ratio values. The *SD* ratio values of the pseudo-first order kinetic model vary from 18.0 to 19.5. The *SD* ratio values of the pseudo-second order model vary from 3.1 to 3.6. Therefore, the adsorption of the pharmaceutical onto rGO is best described by the general order kinetic model that has *SD* ratio value of 1.0.

The half-life ($t_{1/2}$), the time taken to attain 50% of q_e (amount adsorbed at the equilibrium), was obtained by interpolation of the kinetic curves. Table 1 presents the $t_{1/2}$ values. Since the general-order kinetic model is the best model that explains kinetic data, its $t_{1/2}$ values are meaningful. To verify the time it takes to attain the equilibrium, an interpolation was made on the general-order kinetic model plot for s-DCF. In this calculation, the value of q_t that was 95% of the maximum value of experimental q_t was used. For s-DCF pharmaceutical, the $t_{0.95}$ ranged from 108.0 to 175.8 min. For continuing the other experiments on adsorption of s-DCF onto rGO, the contact time of 200 min was used. The contact time was increased to ensure that equilibrium is attained between the pharmaceutical and the adsorbent at different concentrations of s-DCF[11].

3.2.2 Equilibrium studies

In this work Langmuir,[30] Freundlich[29] and Liu[31] isotherm models were utilized to analyze the isothermal data. The isothermal experiments were investigated at 25 ^{o}C with a contact time of 200 min between the adsorbent and adsorbate, mass of adsorbent of 30.0 mg, pH of s-DCF solution fixed at 10.0. The adsorption isotherm plot of s-DCF onto rGO at 25^{o}C is presented in Figure 3. Between the Liu model gives the best description of adsorption equilibrium data of s-DCF onto rGO based on the *SD* values (Table 2). The *SD* ratio values of the Langmuir model was 9.1 while the value of Freundlich model was 17.9. The maximum amount (Q_{max} value) of s-DCF removed at 25^{o}C is 59.67 mg g^{-1} for s-DCF. The Q_{max} obtained in this work is within the same magnitude of Q_{max} obtained in the literature for activated carbon[11] and carbon xerogels.[12]

3.2.3 Thermogravimetric analysis of diclofenac adsorbed on rGO

Physical evidence of diclofenac interaction with the rGO was confirmed using thermogravimetric analysis, comparing the thermograms of pure rGO and s-DCF, with the loaded adsorbent (Figure 4). As seen, the curve of pristine rGO shows only the loss mass events related to the presence of functional groups and of carbon skeleton, the curve of s-

DCF shows three events (250 - 380 ºC, 458 - 505 ºC and 573 - 678 ºC), all associated with different oxidation steps of the drug structure.[13] The thermogram of rGO after adsorption, beyond the characteristics mass loss of pure adsorbent, presents two of the loss mass events of diclofenac. Indicating that due to a good interaction between the two components, the s-DCF tends to remain adhered to the graphene, after the centrifugation, even at low surface coverage.

3.3. Theoretical Results

The electronic and structural properties of s-DCF and graphene-family (pristine graphene, graphene with a single vacancy and functionalized graphene, that mimics the rGO used as nanoadsorbent), can be founded on supplementary material (Figures S1 – S6). The nomenclatures used are according to Bianco *et. al.*[43] All those isolated molecules have presented electronic and structural properties in good agreement with results already reported on literature.[37]

3.3.1Graphene-family interacting with s-DCF

To evaluate the interaction between the s-DCF drug with pristine graphene, graphene with a single vacancy and functionalized graphene, different configurations were analyzed for each case. Table 3 and 4 summarizes the values of binding energies, bond distance and charge transfer (Δq) for the most stable configurations. Negative values of E_b and Δq, respectively, indicate that there is an attraction between s-DCF and graphene, and also that drug is charge acceptor. Figures 5 and 6 exhibit the structural conformation (side and top view) for the most stable configurations and Figures 7 and 8, respectively, present the band structure to all configurations above cited.

It is emphasized that according to Dreyer and coworkers[38] hydroxyl and epoxy functional groups was mainly localized on basal plane of graphene, while carboxyl and carbonyl groups lay down in graphene edges. In addition, the methodology involved requires that the graphene simulated possess boundary conditions along two axis, i.e., the graphene

is interpreted like an infinite two-dimensional plane. In that way, this graphene exhibit none edge to attach the carboxyl groups or carbonyl groups. Therefore, to create a border/edge in this simulation it would be through the usage of a nanoribbon (a one-dimensional plane of graphene). From this, to evaluate the interaction between s-DCF drug and carboxyl/carbonyl functionalized graphene, as well as considering edge effects, was adopted a graphene nanoribbon with armchair edges and width of 13 dimers lines (13 AGNR as convention). Moreover, taking into account that greatest binding energies are more relevant to adsorption process, only configurations where the functional groups are in the same side of graphene plane are studied, thus favoring electrostatic interactions between the s-DCF molecule and graphene, increasing the binding energies.

3.3.2. Pristine graphene and graphene plus a single vacancy interacting with s-DCF

As showed on Table 3, the binding energy to pristine graphene interacting with s-DCF is maximum 0.8eV. Machado *et al.*[15] establish a relationship between the enthalpy of the real system and binding energy from theoretical results. From that, they have considered enthalpy values below 80 kJ mol^{-1} (~0.83eV) representative of physical adsorption process. In that way, the interaction between pristine graphene and s-DCF point to physical adsorption regime. The presence of physical adsorption is also supported by lower values of charge transfer and high bond distance, indicating no chemical bonds. As for graphene plus a single vacancy interacting with s-DCF, from an analysis of binding distance, charge transfer, and optimized molecular structure of the system, no significant changes, compared to the same configuration without vacancy, can be found. Indeed the molecular structure before and after s-DCF adsorption, for pristine or single vacancy graphene, are quite similar (Figures 5a and 5b, respectively) indicating that even in with a single vacancy on basal graphene plane, a physical adsorption regime prevails. However the binding energy to s-DCF adsorbed on graphene plus a vacancy is larger than from pristine one (Table 3 (a) and (b)). This can be assigned to possible electrostatic interactions between mismatched charges in graphene plus a vacancy and the ion Na^{+}, located just above the vacancy. Thus,

comparing pristine graphene versus graphene plus a vacancy, it is observed that electrostatic interactions contribute to an increase in overall binding energy. Similar results were founded by other researchers[44-46] where was verified that the presence of vacancies in graphene basal plane contribute to increasing the binding energies between a molecule and graphene. Moreover we founded that the most stable structures in both cases are that ones where the drug maintain a larger number of hexagonal carbon rings over graphene rings, forming a Bernal stacking, increasing the surface area and favoring π-π interactions between graphene and s-DCF.

From band structure to both s-DCF being adsorbed on pristine graphene or on graphene plus a vacancy (Figures 7(a) and 7(b), respectively), one can notice just an overlap of graphene levels with s-DCF levels, without hybridization or combination of these levels, especially if looking above Fermi level. Once again, a single vacancy do not modify the characteristic of s-DCF adsorption on graphene, therefore to this two configurations one can conclude that the s-DCF drug interact weakly with graphene, characteristic of a physical adsorption regime.

3.3.3. Epoxy and hydroxyl functionalized graphene interacting with s-DCF

Figures 5 (c), (d), (e) and (f), exhibit the most stable conformations to epoxy and hydroxyl functionalized graphene interacting with s-DCF. To optimized configurations, comparing epoxy functionalized graphene, Figures 5 (c), (d), versus hydroxyl functionalized graphene, Figures 5 (e) and (f), the s-DCF molecule do not stay on a planar conformation over graphene to the last ones. This two distinct conformations reveals a difference on type of interaction drug-graphene in each case. A possible formation of hydrogen bonds at expense of π-π ones could cause such conformational differences. Nan and coworkers[10], though the molecular modeling, suggest that diclofenac interact with GO through hydrophobic and π-π interactions. However, the GO studied by these authors has no functional groups on their surface. Thus, the hydrogen bonds who plays a important hole on adsorption of s-DCF on rGO have been neglected.

Comparing the biding energies values to graphene without any functional groups (Table 3 (a) and (b)) versus the functionalized graphene by one or two epoxy groups (Table 3 (c) and (d)) it is noticeable a larger biding energy to the last ones. Moreover, unlike for pristine graphene to functionalized graphene with epoxy groups, the most stable configuration occur when the possibility for the formation of hydrogen bonds are higher, due to the cost of π-π interactions between graphene and s-DCF drug. Thus, these imply in a significant modification on the type of the occurring interactions. Nevertheless, if a comparison was made between the band levels to isolate epoxy functionalized graphene (Figures S4(a) and S4(b)), versus s-DCF adsorbed on epoxy functionalized graphene (Figures 7(c) and 7(d)), it is noticeable that even for s-DCF adsorbed on epoxy functionalized graphene, the shape of band levels near Fermi level do not undergo any significant change. Thus, a presence of epoxy groups on the basal plane of graphene maintain a physical adsorption regime to s-DCF adsorption.

Similarly to occurs to epoxy functionalized graphene, if making a comparison between binding energies on Table 3, to configurations involving graphene without any functionalization (a), (b) with hydroxyl functionalized graphene (e), (f), respectively, one can observe that binding energies to hydroxyl functionalized graphene are greater than no functionalized ones. Furthermore, as showed on Table 3, the binding energies between s-DCF molecule and hydroxyl functionalized graphene are still higher than to configurations involving epoxy functionalized graphene. Bond distances to hydroxyl functionalized graphene was smaller than epoxy functionalized graphene, wherein the shortest distance occurs between the hydroxyl groups and R-O drug radical. Such observations reveals that hydrogen bonds have preponderant contribution to binding energies between s-DCF and hydroxyl functionalized graphene, while π-π or electrostatic interactions are secondary.

Comparing band levels to isolate hydroxyl functionalized graphene (Figure S5 (a) and S5(b)), with s-DCF adsorbed on hydroxyl functionalized graphene (Figure 7(e) and 7(f)), no significant variation in their band levels can be notice, whether above (conduction band) neither below (valence band). Either to one or two hydroxyl groups, only a presence of a flat

level, just below the Fermi level, from s-DCF molecule appears overlapped to graphene levels. This observation again provides an indication of the weak interaction between graphene and the s-DCF drug, characteristics of a physisorption regime.

3.3.4. Carboxyl and carbonyl functionalized graphene nanoribbons interacting with s-DCF

Carboxyl functionalized graphene nanoribbons interacting with s-DCF exhibit greater binding energy among all other studied configurations on this paper (see on Table 4). Also comparing on same table the binding energies between one-carboxylated nanoribbon interacting with s-DCF versus two-carboxylated nanoribbon, it is possible to observe that the last one exhibit an increase on binding energy around 1,3 eV. Moreover, a greater charge transfer and smallest binding distance to s-DCF molecule adsorbed on two-carboxylated nanoribbon configuration, indicates a predominance of strong interactions among these molecules by hydrogen bonds. Therefore, the binding energy increase as the number of sites available for this type of interaction also increases. In particular is remarkable that most stable configurations occur when the drug do not donate charge to nanoribbon, i.e. even in a presence of hydrogen bonding, binding energies trend to stay lower if the charge transfer occurs from drug to nanoribbon.

From Figures 6 (a) and (b) it is possible to note that the adsorption of s-DCF drug on carboxyl functionalized graphene nanoribbons leads to a significant deformation or bending on nanoribbon edge, thus again indicating a occurrence of hydrogen bonding between hydroxyl groups and s-DCF drug. This bending on nanoribbon edge also can be observed to s-DCF drug adsorbed on carbonyl functionalized graphene nanoribbons (Figures 6 (c) and 6(d)) though less significantly.

As can be compared by band structure to isolate carboxyl functionalized graphene nanoribbons (Figure S6 (a) and S6(b)), versus carboxyl functionalized graphene nanoribbons interacting with s-DCF (Figure 8 (a) and 8(b)), the adsorption of s-DCF molecule did not modify significantly the electronic structure of nanoribbons. In both cases (to one or two-carboxyl groups) the energy levels of s-DCF molecule remain overlapped to nanoribbon

levels without hybridization or interlacement between these levels. Small changes on band structure only can be noted to s-DCF molecule interacting with one carboxylated nanoribbon, where few levels below valence band appear distorted comparing after with before s-DCF adsorption on nanoribbon. This level distortion however does not seems caused to s-DCF molecule adsorption on nanoribbon since both binding energy and charge transfer for this configuration are smaller than for two carboxylated nanoribbon. Instead, this small change below valence band levels may be attributed to structural deformation of nanoribbon after adsorption, since nanoribbon presents a significant bend on its structure at the site where is located the carboxyl group, thus losing its planar conformation (Figures 6(a) and 6(b)).

To carbonyl functionalized graphene nanoribbons interacting with s-DCF, unlike to carboxylated ones, the nanoribbons trends to keep the planar conformation (Figure 6 (c), and 6(d)), allowing a greater approach of s-DCF molecule to nanoribbon plane. Thus, hydrogen bonding on these configurations turns equally effective, in terms of intensity of binding, when comparing to π-π interactions plus electrostatic bonds between the carbonyl group and the sodium ion. In other words, the total binding energy to carbonyl functionalized graphene nanoribbons interacting with s-DCF is mainly composed by a half due hydrogen bonding and the other half due π-π interactions plus electrostatic forces.

The band structure to one carbonyl functionalized graphene nanoribbon after s-DCF adsorption (Figure 8 (c)) shows a straight/flat level just below the Fermi level, presenting a donor character. Meanwhile for nanoribbon with two carbonyl groups (Figure 8 (d)), the straight/flat level appears double, thus indicating a presence of a small spin polarization in this last case. In addition, the adsorption of s-DCF molecule on these nanoribbons adds additional flat levels below the valence level, but just overlapping ribbons levels, thus indicating a small interaction between s-DCF levels with sp^2 orbitals of nanoribbons. Furthermore, analyzing band levels near the Fermi level, s-DCF adsorption on nanoribbons leads to a downgrade of the previous semi-occupied and hybridized ribbon level, indicating that the carbonyl functional group is receiving or sharing charge instead donating.

4. Conclusions

In this work adsorption experiments was conducted to evaluate the sorption capacity of rGO for removing s-DCF drug from aqueous solutions. Thus from experimental studies three kinetic models were used to adjust the adsorption and the best fit was obtained with the general-order kinetic model. The equilibrium isotherm of the s-DCF drug was obtained, and these data were best fit to the Liu isotherm model. The maximum adsorption capacity for rGO was 59.67 mg g^{-1} at 25 ^{o}C. First principles calculations based on DFT and implemented by SIESTA code were performed to evaluate the interaction between s-DCF molecule and graphene-family, as well as experimental studies in order to assess the graphene batch adsorption capacity. Thus, from computer simulations it was found that interactions between pristine graphene and s-DCF can be classified as physical adsorption process, as no significant structural and/or electronic changes after s-DCF adsorption could be noted. To pristine graphene and graphene plus a single vacancy, the most stable configurations are those ones where the s-DCF present hexagonal carbon rings over graphene rings forming a Bernal like stacking, thus indicating a predominance of π-π interactions.

Regarding the adsorption of s-DCF molecule on functionalized graphene or nanoribbons, binding energies trend to increases as number of functional groups increase. Moreover, the most relevant interaction in terms of binding energy can be attributed to hydrogen bonding. The intensity of binding energies in relation to presence of functional groupson graphene surface follows the order carboxyl > hydroxyl > carbonyl > epoxy. These results are promising because they provide a evidence as how occurs the s-DCF adsorption on graphene. Furthermore, was demonstrated that in general there is a physical adsorption of s-DCF on graphene, which is desired as could provide desorption of these contaminants thus enabling the reuse of graphene.

From this scenario, experimental adsorption experiments and *ab initio* calculations point out that graphene-family are promising materials for adsorption and removal of s-DCF from aqueous solutions.

Acknowledgements

The authors thanks to CNPq, CAPES and INCT Nanocarbono for financial support, to Centro Nacional de Processamento de Alto Desempenho (CENAPAD - SP) for computational support and LACTEC for BET measurements.

References

1. K. Kümmerer, *Journal of Antimicrobial Chemotherapy*, 2004, **54**, 311-320.
2. J. Lienert, K. Güdel and B. I. Escher, *Environmental science & technology*, 2007, **41**, 4471-4478.
3. W. Gebhardt and H. F. Schröder, *Journal of Chromatography A*, 2007, **1160**, 34-43.
4. K. Dutta, M.-Y. Lee, W. W.-P. Lai, C. H. Lee, A. Y.-C. Lin, C.-F. Lin and J.-G. Lin, *Bioresource technology*, 2014, **165**, 42-49.
5. D. C. dos Santos, M. A. Adebayo, S. d. F. P. Pereira, L. D. T. Prola, R. Cataluña, E. C. Lima, C. Saucier, C. R. Gally and F. M. Machado, *Korean Journal of Chemical Engineering*, 2014, **31**, 1470-1479.
6. L. H. Santos, A. N. Araújo, A. Fachini, A. Pena, C. Delerue-Matos and M. Montenegro, *Journal of hazardous materials*, 2010, **175**, 45-95.
7. P. Verlicchi, M. Al Aukidy and E. Zambello, *Science of the Total Environment*, 2012, **429**, 123-155.
8. N. Vieno and M. Sillanpää, *Environment international*, 2014, **69**, 28-39.
9. M. E. DeLorenzo and J. Fleming, *Archives of environmental contamination and toxicology*, 2008, **54**, 203-210.
10. S.-W. Nam, C. Jung, H. Li, M. Yu, J. R. Flora, L. K. Boateng, N. Her, K.-D. Zoh and Y. Yoon, *Chemosphere*, 2015, **136**, 20-26.
11. C. Saucier, M. A. Adebayo, E. C. Lima, R. Cataluña, P. S. Thue, L. D. Prola, M.

544 Puchana-Rosero, F. M. Machado, F. A. Pavan and G. Dotto, *Journal of hazardous*
545 *materials*, 2015, **289**, 18-27.
546 12. N. Suriyanon, P. Punyapalakul and C. Ngamcharussrivichai, *Chemical Engineering*
547 *Journal*, 2013, **214**, 208-218.
548 13. D. Krajišnik, A. Daković, A. Malenović, L. Djekić, M. Kragović, V. Dobričić and J. Milić,
549 *Microporous and Mesoporous Materials*, 2013, **167**, 94-101.
550 14. J. L. Sotelo, G. Ovejero, A. Rodríguez, S. Álvarez, J. Galán and J. García, *Chemical*
551 *Engineering Journal*, 2014, **240**, 443-453.
552 15. F. M. Machado, C. P. Bergmann, E. C. Lima, B. Royer, F. E. de Souza, I. M. Jauris, T.
553 Calvete and S. B. Fagan, *Physical Chemistry Chemical Physics*, 2012, **14**, 11139-11153.
554 16. L. D. Prola, F. M. Machado, C. P. Bergmann, F. E. de Souza, C. R. Gally, E. C. Lima, M.
555 A. Adebayo, S. L. Dias and T. Calvete, *Journal of environmental management*, 2013,
556 **130**, 166-175.
557 17. M. C. Ribas, M. A. Adebayo, L. D. Prola, E. C. Lima, R. Cataluña, L. A. Feris, M.
558 Puchana-Rosero, F. M. Machado, F. A. Pavan and T. Calvete, *Chemical Engineering*
559 *Journal*, 2014, **248**, 315-326.
560 18. F. M. Machado, C. P. Bergmann, T. H. Fernandes, E. C. Lima, B. Royer, T. Calvete and
561 S. B. Fagan, *Journal of hazardous materials*, 2011, **192**, 1122-1131.
562 19. S. Chowdhury and R. Balasubramanian, *Advances in colloid and interface science*,
563 2014, **204**, 35-56.
564 20. C. P. Bergmann and F. M. Machado, *Carbon Nanomaterials as Adsorbents for*
565 *Environmental and Biological Applications*, Springer, 2015.
566 21. L. A. Al-Khateeb, S. Almotiry and M. A. Salam, *Chemical Engineering Journal*, 2014,
567 **248**, 191-199.
568 22. S.-T. Yang, S. Chen, Y. Chang, A. Cao, Y. Liu and H. Wang, *Journal of colloid and*
569 *interface science*, 2011, **359**, 24-29.
570 23. Y. Li, Q. Du, T. Liu, X. Peng, J. Wang, J. Sun, Y. Wang, S. Wu, Z. Wang and Y. Xia,
571 *Chemical Engineering Research and Design*, 2013, **91**, 361-368.

572 24. Y. Gao, Y. Li, L. Zhang, H. Huang, J. Hu, S. M. Shah and X. Su, *Journal of colloid and*
573 *interface science*, 2012, **368**, 540-546.
574 25. J. Xu, L. Wang and Y. Zhu, *Langmuir*, 2012, **28**, 8418-8425.
575 26. P. Hohenberg and W. Kohn, *Physical Review*, 1964, **136**, B864.
576 27. W. Kohn and L. J. Sham, *Physical Review*, 1965, **140**, A1133-A1138.
577 28. H. Mehl, C. F. Matos, E. G. Neiva, S. H. Domingues and A. J. Zarbin, *Quim. Nova*, 2014,
578 **37**, 1639-1645.
579 29. H. M. F. Freundlich, *Zeitschrift für Physikalische Chemie*, 1906, **57**, 385-470.
580 30. I. Langmuir, *Journal of the American Chemical society*, 1918, **40**, 1361-1403.
581 31. Y. Liu, H. Xu, S.-F. Yang and J.-H. Tay, *Journal of biotechnology*, 2003, **102**, 233-239.
582 32. D. C. dos Santos, M. A. Adebayo, E. C. Lima, S. F. Pereira, R. Cataluña, C. Saucier, P.
583 S. Thueb and F. M. Machadoe, *J. Braz. Chem. Soc*, 2015, **26**, 924-938.
584 33. J. M. Soler, E. Artacho, J. D. Gale, A. García, J. Junquera, P. Ordejón and D. Sánchez-
585 Portal, *Journal of Physics: Condensed Matter*, 2002, **14**, 2745.
586 34. N. Troullier and J. L. Martins, *Physical Review B*, 1991, **43**, 1993-2006.
587 35. S. Boys and F. d. Bernardi, *Molecular Physics*, 1970, **19**, 553-566.
588 36. X. Ren et al., Dalton Trans 2013, **42**, 5266–5274.
589 37. G.K. Ramesha et al., J Colloid Interface Sci , 2011, **361**, 270–277.
590 38. J.M. Kim et al, Int J Hydrogen Energ, 2014, **39**, 3799–3804.
591 39. S. Liu et al., Appl Surf Sci, 2012, **258**, 5299–5303.
592 40. W. Chen, L. Yan and P. R. Bangal, *Carbon*, 2010, **48**, 1146-1152.
593 41. F. Banhart, J. Kotakoski and A. V. Krasheninnikov, *ACS Nano*, 2010, **5**, 26-41.
594 42. D. R. Dreyer, S. Park, C. W. Bielawski and R. S. Ruoff, *Chemical Society Reviews*,
595 2010, **39**, 228-240.
596 43. A. Bianco, H.-M. Cheng, T. Enoki, Y. Gogotsi, R. H. Hurt, N. Koratkar, T. Kyotani, M.
597 Monthioux, C. R. Park and J. M. Tascon, *Carbon*, 2013, **65**, 1-6.
598 44. Y.-H. Zhang, Y.-B. Chen, K.-G. Zhou, C.-H. Liu, J. Zeng, H.-L. Zhang and Y. Peng,
599 *Nanotechnology*, 2009, **20**, 185504.

45. Y.-n. Guo, X. Lu, J. Weng and Y. Leng, *The Journal of Physical Chemistry C*, 2013, **117**, 5708-5717.
46. D. Dutta, B. C. Wood, S. Y. Bhide, K. G. Ayappa and S. Narasimhan, *The Journal of Physical Chemistry C*, 2014, **118**, 7741-7750.

Figure captions.

Figure 1. (a) SEM image; (b) AFM image and height profiles; (c) FT-IR spectrum (of GO and rGO) (d) TGA curves at air atmosphere and (e) Raman spectrum of the reduced graphene oxide used as nanoadsorbent.

Figure 2. Kinetics of adsorption of s-DCF onto rGO. (a) 40.0 mg L^{-1} s-DCF; (b) 70.0 mg L^{-1} s-DCF. Temperature was fixed at 25^{o}C, mass of adsorbent fixed at 30.0 mg and pH of s-DCF fixed at 10.0.

Figure 3. Isotherm of adsorption of s-DCF onto rGO. Conditions: temperature was fixed at 25^{o}C mass of adsorbent 30.0 mg, time of contact between the s-DCF and rGO was 200 min; pH of s-DCF 10.0.

Figure 4. TGA curves in air of rGO (black), s-DCF (blue) and loaded rGO after adsorption process (red).

Figure 5. Optimized structures to: (a) pristine graphene + s-DCF, (b) graphene plus vacancy + s-DCF, (c) graphene + 1epoxy + s-DCF, (d) graphene + 2epoxy + s-DCF, (e) graphene + 1hidroxyl + s-DCF, (f) graphene + 2hidroxyl + s-DCF.

Figure 6. Optimized structures to: (a) nanoribbon + 1carboxyl + s-DCF, (b) nanoribbon + 2carboxyl + s-DCF, (c) nanoribbon + 1carbonyl + s-DCF, (d) nanoribbon + 2carbonyl + s-

628 DCF.

629

630 **Figure 7.** Band structure to optimized configurations: (a) pristine graphene + s-DCF, (b)
631 graphene plus vacancy + s-DCF, (c) graphene + 1epoxy + s-DCF, (d) graphene + 2epoxy +
632 s-DCF, (e) graphene + 1hidroxyl + s-DCF, (f) graphene + 2hidroxyl + s-DCF.

633

634 **Figure 8.** Band structure to optimized configurations: (a) nanoribbon + 1carboxyl + s-DCF,
635 (b) nanoribbon + 2carboxyl + s-DCF, (c) nanoribbon + 1carbonyl + s-DCF, (d) nanoribbon +
636 2carbonyl + s-DCF.

637 **Table 1**. Kinetic parameters of s-DCF anti-inflammatory adsorption onto rGO. Conditions:
638 temperature, 25°C; pH,10.0; mass of adsorbent, 30.0 mg.

	40.0 mg L^{-1}	**70.0 mg L^{-1}**
Pseudo-first-order		
k_1 (min^{-1})	0.1241	0.1788
q_e (mg g^{-1})	21.52	32.63
$t_{1/2}$ (min)	5.584	3.878
R^2_{adj}	0.9514	0.9536
SD (mg g^{-1})	1.275	1.796
Pseudo-second-order		
k_2 (g mg^{-1} min^{-1})	$9.067.10^{-3}$	$8.709.10^{-3}$
q_e (mg g^{-1})	22.64	34.16
$t_{1/2}$ (min)	4.871	3.362
R^2_{adj}	0.9983	0.9986
SD(mg g^{-1})	0.2383	0.3129
General-order		
k_N [min^{-1}.(g mg^{-1})$^{n-1}$]	$3.381.10^{-3}$	$3.388.10^{-3}$
q_e (mg g^{-1})	23.24	34.81
N	2.350	2.302
$t_{1/2}$ (min)	4.859	3.268
$t_{0.95}$ (min)	175.8	108.0
R^2_{adj}	0.9999	0.9999
SD(mg g^{-1})	0.06529	0.09983

639

640

641 **Table 2.** Isotherm parameters of s-DCF adsorption using rGO. Conditions: pH, 10.0
642 adsorbent mass, 30.0 mg; contact time, 200 min, temperature 25°C.

Langmuir	
Q_{max} (mg g^{-1})	69.41
K_L (L mg^{-1})	0.1048
R^2_{adj}	0.9618
SD(mg g^{-1})	3.750
Freudlich	
K_F (mg g^{-1} (mg L^{-1})$^{-1/n_F}$)	18.83
n_F	3.571
R^2_{adj}	0.8517
SD(mg g^{-1})	7.384
Liu	
Q_{max}(mg g^{-1})	59.67
K_g (L mg^{-1})	0.1267
n_L	1.928
R^2_{adj}	0.9995
SD (mg g^{-1})	0.4121

643

644

645 **Table 3.** Values of binding distance (d_b), binding energies (E_b) and charge transfer (Δq) for
646 graphene interacting with s-DCF in different configurations.

Configuration	d_b(Å)	E_b(eV)	Δq (e^-)
(a) Grap (pristine) + s-DCF	C_{grap} – H = 2.56	-0.800	-0.086
(b) Grap (vacancy) + s-DCF	C_{grap} – H = 2.53	-1.010	0.029
(c) Grap + 1epoxy + s-DCF	O_{grap} – Na = 2.27	-1.213	-0.066
(d) Grap + 2epoxy + s-DCF	O_{grap} – Na = 2.23	-1.407	-0.086
(e) Grap + 1hidroxyl + s-DCF	H_{grap} – O = 1.52	-1.347	0.120
(f) Grap + 2hidroxyl + s-DCF	H_{grap} – O = 1.74	-1.850	0.006

647

648

649 **Table 4.** Values of binding distance (d_b), binding energies (E_b) and charge transfer (Δq) for
650 graphene nanoribbon interacting with s-DCF in different configurations.

Configuration	d_b(Å)	E_b(eV)	Δq (e^-)
(a) Ribbon + 1carboxyl + s-DCF	H_{grap} – O = 1.34	-2.245	0.296
(b) Ribbon + 2carboxyl + s-DCF	H_{grap} – O = 1.15	-3.558	0.438
(c) Ribbon + 1carbonyl + s-DCF	H_{grap} – O = 2.15	-1.481	0.075
(d) Ribbon + 2carbonyl + s-DCF	O_{grap} – Na = 2.15	-1.403	0.130

651

652

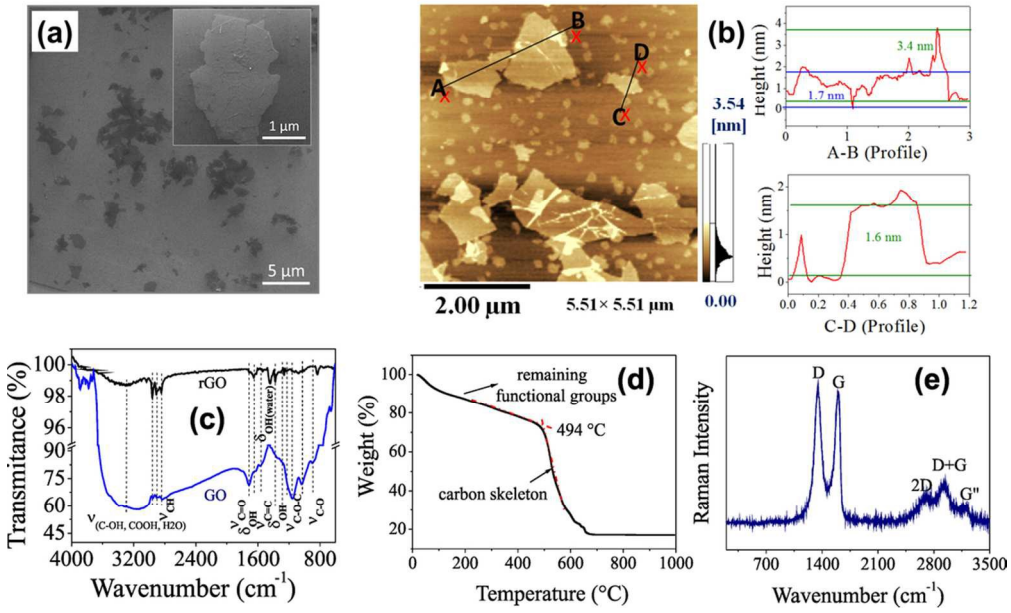

94x57mm (300 x 300 DPI)

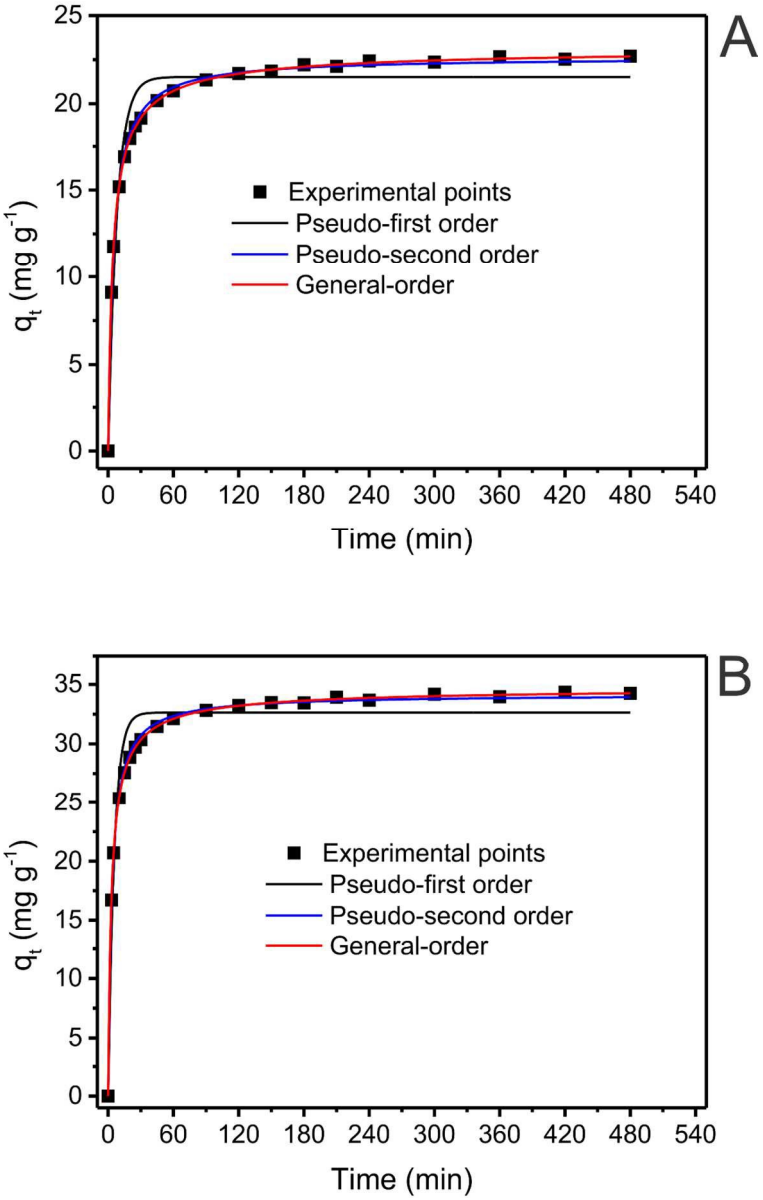

64x102mm (600 x 600 DPI)

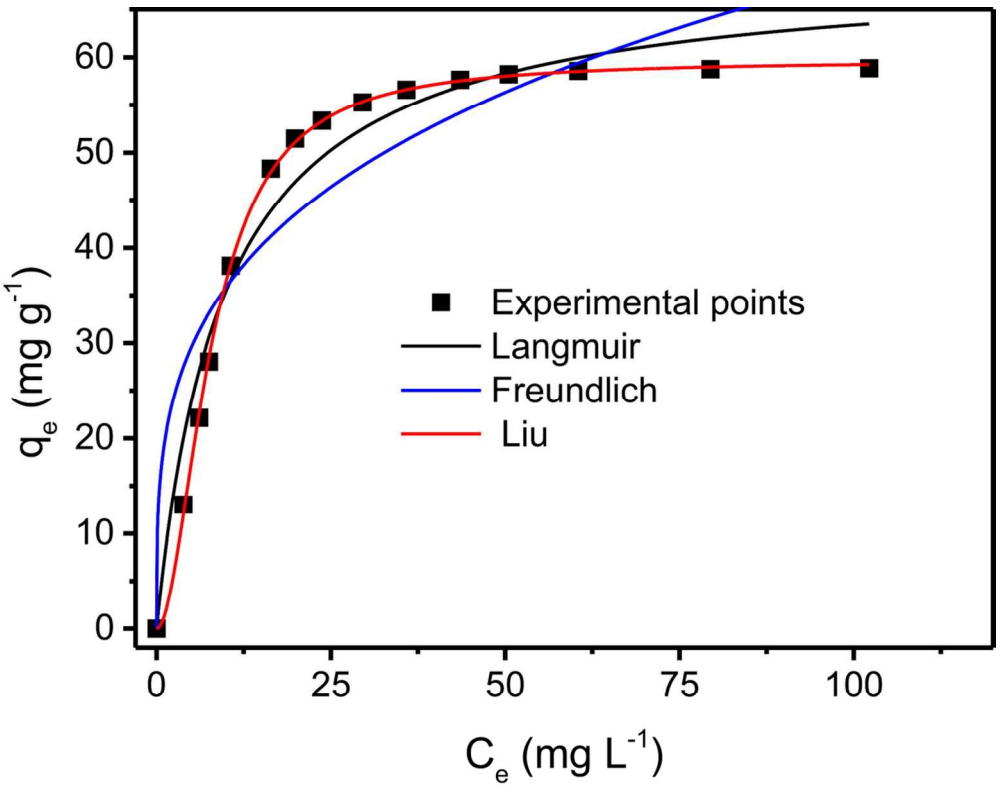

54x42mm (600 x 600 DPI)

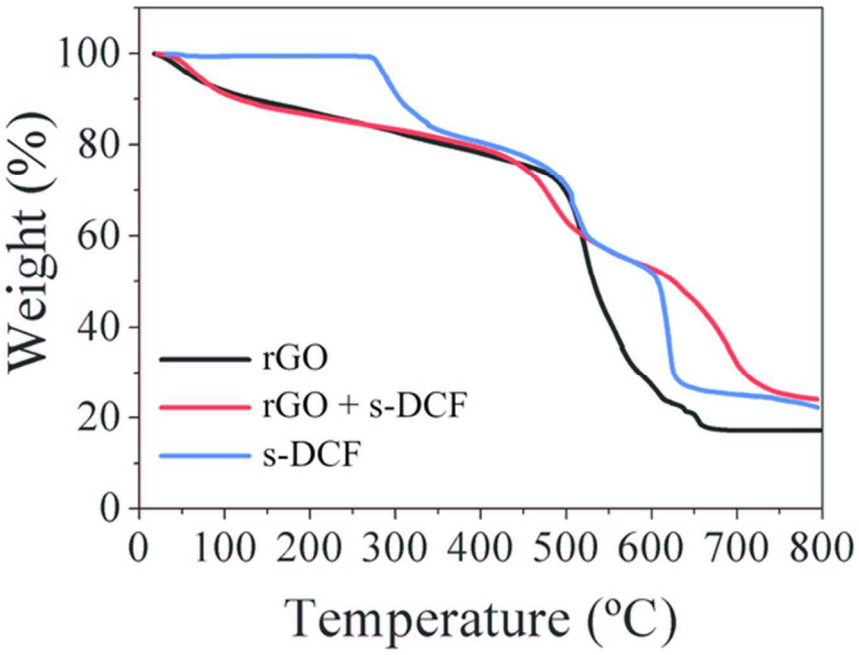

57x40mm (300 x 300 DPI)

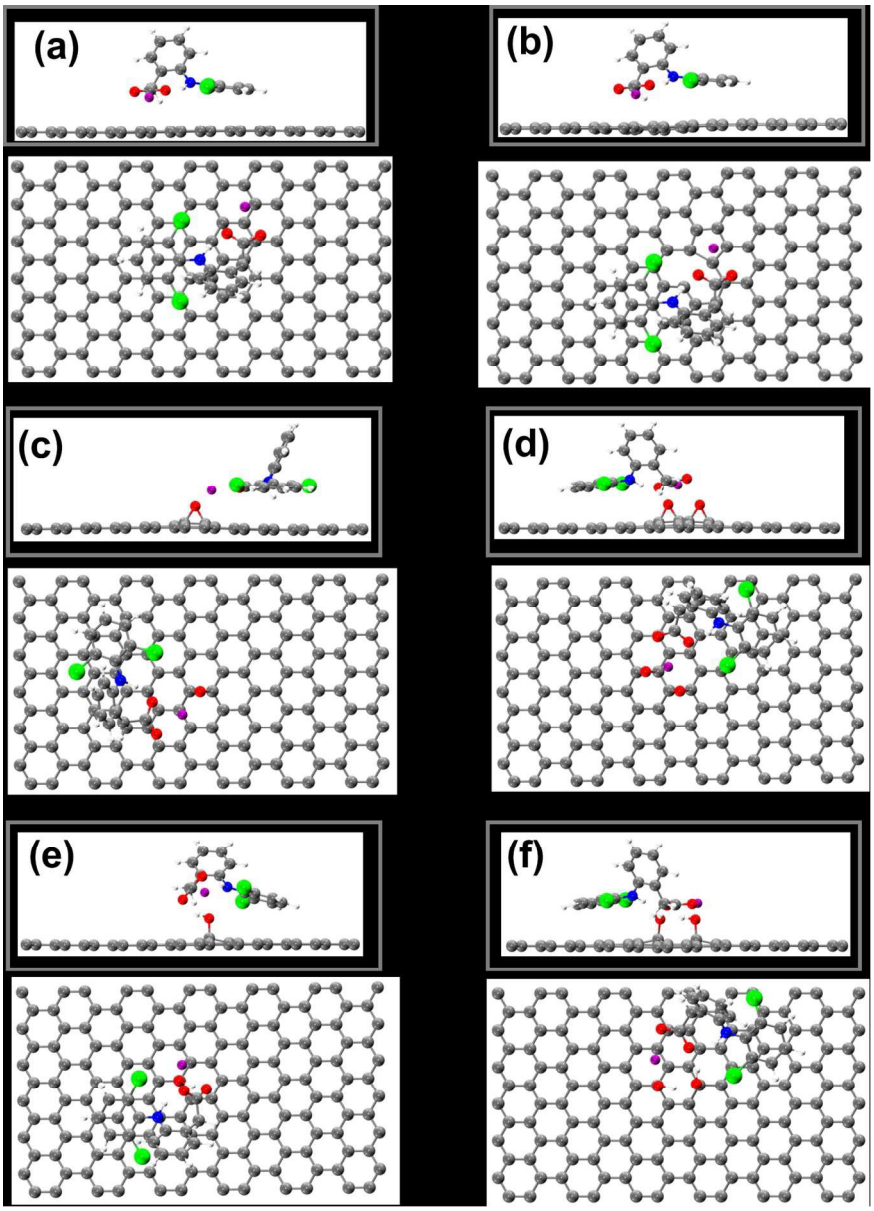

132x184mm (300 x 300 DPI)

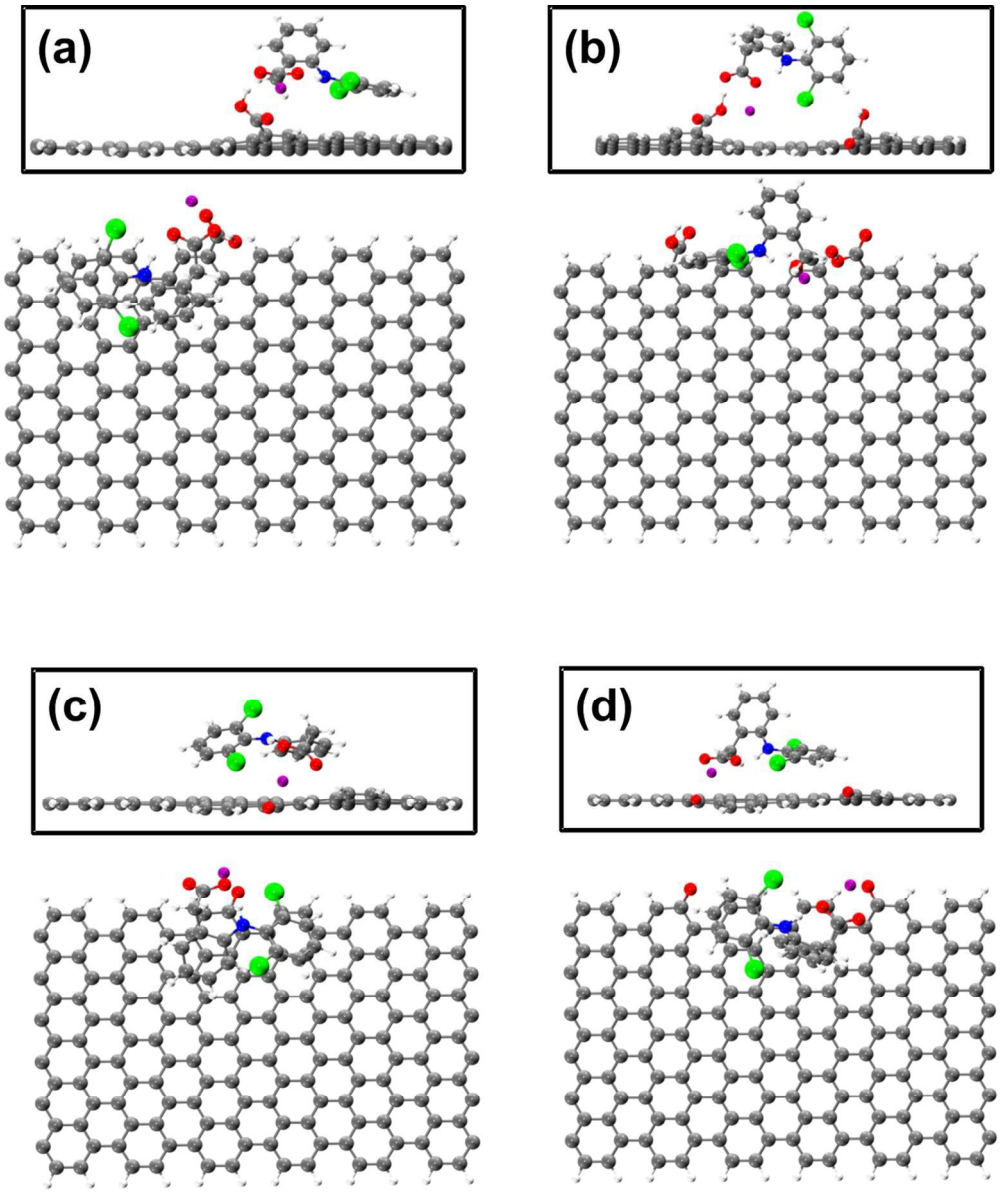

121x144mm (300 x 300 DPI)

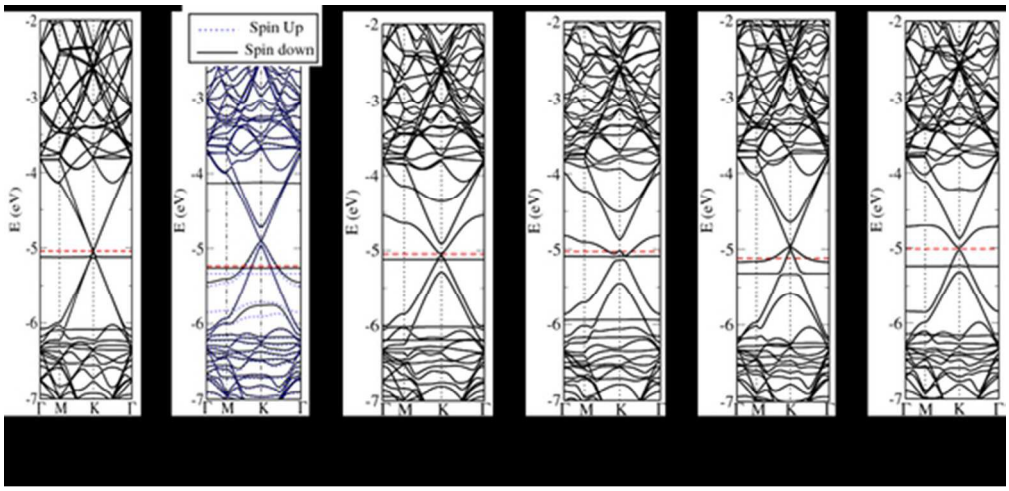

49x23mm (300 x 300 DPI)

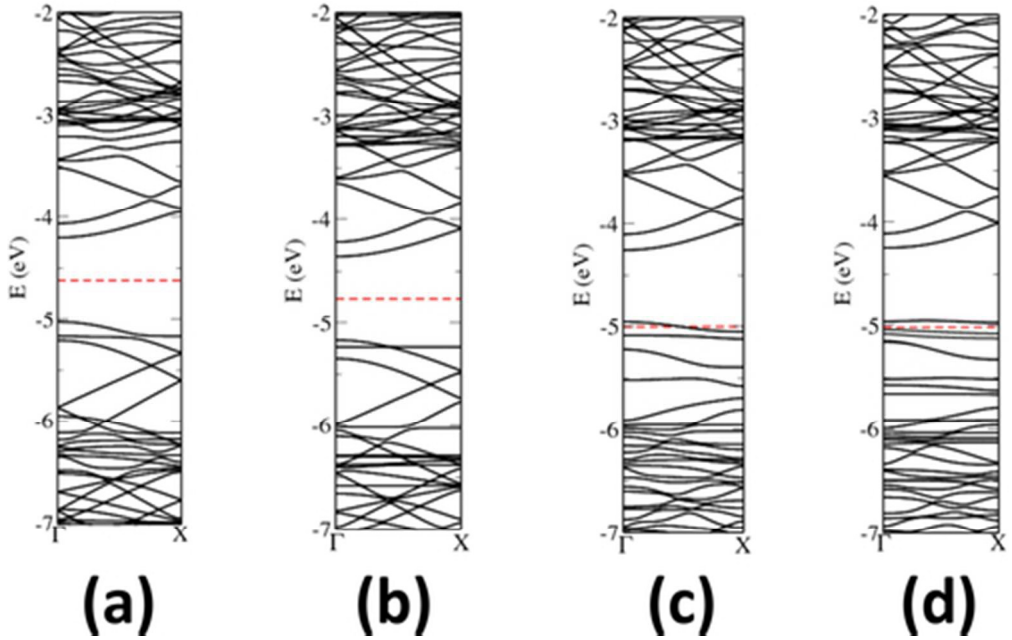

42x27mm (300 x 300 DPI)